



# Catalytic Ozonation of Nitrobenzene by Manganese-Based Y Zeolites

Jingze Hu<sup>1</sup>, Yiming Li<sup>1</sup>, Shaoshuai Nan<sup>1</sup>, Brandon A. Yoza<sup>2</sup>, Yifan Li<sup>1</sup>, Yali Zhan<sup>1</sup>, Qinghong Wang<sup>1</sup>, Qing X. Li<sup>3</sup>, Shaohui Guo<sup>1</sup> and Chunmao Chen<sup>1\*</sup>

<sup>1</sup> State Key Laboratory of Petroleum Pollution Control, China University of Petroleum-Beijing, Beijing, China, <sup>2</sup> Hawaii Natural Energy Institute, University of Hawaii at Manoa, Honolulu, HI, United States, <sup>3</sup> Department of Molecular Biosciences and Bioengineering, University of Hawaii at Manoa, Honolulu, HI, United States

Catalytic ozonation process (COP) is considered as a cost-efficient technology for the treatment of refractory chemical wastewaters. The catalyst performance plays an important role for the treatment efficiency. The present study investigated efficiencies and mechanisms of manganese (Mn)-based Y zeolites in COPs for removing nitrobenzene from water. The catalysts of Mn/NaY and Mn/USY were prepared by incipient wetness impregnation, while Mn-USY was obtained by hydrothermal synthesis. Mn-USY contained a greater ratio of Mn<sup>2+</sup> than Mn/NaY, and Mn/USY. Mn oxides loaded on Y zeolites promoted the COP efficiencies. Mn/NaY increased total organic carbon removal in COP by 7.3% compared to NaY, while Mn/USY and Mn-USY increased 11.5 and 15.8%, respectively, relative to USY in COP. Multivalent Mn oxides (Mn<sup>2+</sup>, Mn<sup>3+</sup>, and Mn<sup>4+</sup>) were highly dispersed on the surface of NaY or USY, and function as catalytic active sites, increasing mineralization. Mn-USY showed the highest total organic carbon removal (44.3%) in COP among the three catalysts, because Mn-USY had a higher ratio of Mn<sup>2+</sup> to the total Mn oxides on the surface than Mn/NaY and Mn/USY and the catalytic effects from intercorrelations between Mn oxides and mesoporous surface structures. The hydroxyl radicals and superoxide radicals governed oxidations in COP using Mn-USY. Nitrobenzene was oxidized to polyhydroxy phenol, polyhydroxy nitrophenol, and p-benzoquinone. The intermediates were then oxidized to small organic acids and ultimately carbon dioxide and water. This study demonstrates the potential of Y zeolites used in COP for the treatment of refractory chemical wastewaters.

**Keywords:** ozonation, catalytic ozonation, Y zeolites, Mn oxides, wastewater treatment

## OPEN ACCESS

### Edited by:

Renato Falcão Dantas,  
Campinas State University, Brazil

### Reviewed by:

Zhihua Xu,  
Jiangnan University, China  
Aihua Xu,  
Wuhan Textile University, China

### \*Correspondence:

Chunmao Chen  
c.chen@cup.edu.cn;  
chunmaochan@163.com

### Specialty section:

This article was submitted to  
Catalysis and Photocatalysis,  
a section of the journal  
Frontiers in Chemistry

**Received:** 14 October 2019

**Accepted:** 24 January 2020

**Published:** 12 February 2020

### Citation:

Hu J, Li Y, Nan S, Yoza BA, Li Y,  
Zhan Y, Wang Q, Li QX, Guo S and  
Chen C (2020) Catalytic Ozonation of  
Nitrobenzene by Manganese-Based Y  
Zeolites. *Front. Chem.* 8:80.  
doi: 10.3389/fchem.2020.00080

## INTRODUCTION

Nitrobenzene is an electrophilic and refractory environmental contaminant that contains a nitro group and a benzene ring. Nitrobenzene is listed as a potential carcinogen by the National Institute of Environmental Health Sciences (Wang and Ma, 2018). Nitrobenzene is removed from water by adsorption (Dasgupta et al., 2018), reduction (Li Y. et al., 2018), and oxidation (El Metwally et al., 2019). The catalytic ozonation process (COP) is widely studied for its application toward the removal of refractory organic chemicals (ROCs) from water. This process is easy to manage, highly efficient, and safe (Chen et al., 2018). The use of catalysts facilitates the decomposition of ozone into highly active species of oxygen, including hydroxyl radicals ( $\cdot\text{OH}$ ), superoxide radicals ( $\text{O}_2^{\cdot-}$ ) and singlet oxygen radicals ( $^1\text{O}_2$ ) (Zhao et al., 2009; Wang et al., 2019). Many catalysts have been previously studied to treat refractory environmental contaminants. Those include

natural minerals (Chen et al., 2015),  $\text{Al}_2\text{O}_3$  and ZSM-5 loaded with metal oxides (Chen et al., 2017, 2018; Xu et al., 2019), and waste sludge biochar (Chen et al., 2019). The use of zeolites catalysts (Nawrocki and Kasprzyk-Hordern, 2010), including those that contain active metallic components (Rosal et al., 2010), have been investigated. However, the catalytic mechanisms that are involved with the degradation of organic chemicals in water remain unclear. ZSM-5 zeolites adsorb ozone and organic molecules onto its surface, promoting proximal reactions (Ikhlaiq et al., 2013). For example, Fe-SBA-15 was found to adsorb oxalic acid, which is then oxidized by radical species (Yan et al., 2016). Acid-treatment of natural zeolite has been determined to promote the removal of methylene blue mainly via  $\cdot\text{OH}$ s mediated oxidation (Valdes et al., 2012).

Dealuminated Y zeolite (USY) was initially recognized as an effective catalyst for use with the COP treatment of phenol (Dong et al., 2008). USY facilitates ozone decomposition and  $\cdot\text{OH}$ s generation (Dong et al., 2008). The Y zeolites possessing a large specific surface area can effectively disperse metal oxides (Vu et al., 2018). While the utilization of Y zeolites for the treatment of volatile organic compounds in gases has been well-documented, little attention has been given to the COP treatment of ROCs in water (Kwong et al., 2008; Einaga et al., 2011). The USY zeolite is produced by the application of an ammonium ion exchange and dealumination by NaY (Sato et al., 1999; Santikunaporn et al., 2004). NaY and USY are differentiated by its textures, structures, and the molar ratio of Si to Al. These differences influence catalytic performance (Sato et al., 2001). To further improve catalytic performance, the surface loading of metallic oxides (Jeirani and Soltan, 2017) such as manganese (Mn) is widely used (Sui et al., 2011; Sun et al., 2014).

In the present study, loadings of Mn oxides on NaY and USY were studied for the catalytic ozonation efficiencies. In addition, Mn loaded Y zeolites (Mn/NaY, Mn/USY, and Mn-USY) were compared with NaY and USY to understand the catalytic mechanisms of the Mn loaded Y zeolites for the reduction of nitrobenzene in water.

## EXPERIMENTAL

### Materials

The NaY zeolite was purchased from Nanjing Xianfeng Nanomaterials Technology Co., Ltd., China. Sodium bicarbonate ( $\text{NaHCO}_3$ ; 99.5 wt.%), ammonium chloride ( $\text{NH}_4\text{Cl}$ ; 99.5 wt.%), manganese nitrate solution ( $\text{Mn}(\text{NO}_3)_2$ ; 50 wt.%) and potassium hydroxide ( $\text{KOH}$ ; 99.5 wt.%) were all obtained from Beijing Chemical Reagents Co., Ltd., Beijing, China. Methanol ( $\text{CH}_3\text{OH}$ ; 99.9 wt.%), p-benzoquinone ( $\text{C}_6\text{H}_4\text{O}_2$ ; 99.5 wt.%) and methylene chloride ( $\text{CH}_2\text{Cl}_2$ ; 99.9 wt.%) were purchased from Fisher Scientific. Inc. 5,5-Dimethyl-1-pyrroline (DMPO) was purchased from Sigma-Aldrich. Inc. Ultrapure water (18.2  $\text{m}\Omega/\text{cm}$ ) was produced by a Direct-Pure UP ultrapure water system (Rephile Shanghai Bioscience Co., Ltd., Shanghai, China).

### Preparation of Catalysts

One hundred grams of NaY was washed by 500 mL of ultrapure water three times and then dried prior to use. Forty grams of

NaY was exchanged using 1 mol/L  $\text{NH}_4\text{Cl}$  solution in a mass ratio of 1:10 (solid-liquid ratio) at an initial pH value at 3–3.5. After stirring at  $90^\circ\text{C}$  for 90 min and filtering, the obtained solid sample was dried at  $90^\circ\text{C}$  for 4 h and calcined at  $550^\circ\text{C}$  for 4 h. After a repeated operation, the USY catalyst was obtained. Mn/NaY and Mn/USY were prepared according to the incipient wetness impregnation method. Briefly, an aliquot of 1.3 mL of 50 wt.%  $\text{Mn}(\text{NO}_3)_2$  solution was added to 8.0 g water followed by impregnation of 10 g NaY or USY, then dried at  $90^\circ\text{C}$  for 4 h and calcined at  $550^\circ\text{C}$  for 4 h. Mn-USY was obtained by hydrothermal synthesis.  $\text{Mn}(\text{NO}_3)_2$  and  $\text{CO}(\text{NH}_2)_2$  were blended in a molar ratio of 1:4 in 20 mL deionized water. This mixture was further blended with 10 g of USY and stirred at  $80^\circ\text{C}$  for 90 min and then the sample was placed in a crystallization kettle and heated to  $100^\circ\text{C}$  for 4 h under slow rotation. Afterwards, the sample was filtered, washed, dried, and calcined at  $550^\circ\text{C}$  for 4 h. Mn oxides ( $\text{MnO}_x$ ) were synthesized according to the same procedure, but without USY. The contents of Mn on Mn-based Y zeolites were detected by ICP-AES. 0.1 g of catalyst was dissolved in a mixture of 5 mL  $\text{HNO}_3$  and 1 mL HF, and saturated  $\text{H}_3\text{BO}_3$  solution was added to eliminate the interference of  $\text{F}^-$ . The three zeolites (Mn/NaY, Mn/USY, and Mn-USY) contained a similar content (3.0 wt.%) of Mn.

### Characterization of Catalysts

X-ray powder diffraction (XRD) was recorded on XRD-6000 powder diffraction instrument (Shimadzu, Kyoto, Japan) with a 40.0 kV working voltage and 40.0-mA electric current. Crystallinities of the Y samples were calculated from the eight defined peak areas ( $2\theta = 15.6, 18.6, 20.3, 23.6, 27.0, 30.7, 31.3, \text{ and } 34^\circ$ ) with the NaY standard sample as a reference according to the ASTM standards (D3906-03). The pore structures were determined with an ASAP 2000 accelerated surface area and porosimetry system (Micromeritics, Norcross, GA, USA). An Inductively Coupled Plasma-Atomic Emission Spectrometer (ICP-AES) (Perkin Elmer DV7000, Waltham, MA, USA) was used for determining the actual Mn content in Mn-based Y zeolites. X-ray photoelectron spectroscopy (XPS) results were obtained on a PHI Quantera SXM photoelectron spectrometer (ULVAC-PHI, Chanhassen, MN, USA) using Al K $\alpha$  radiation ( $h\nu = 1486.6\text{ eV}$ ). The binding energy (BE) values were referred to the C1s line at 284.8 eV. Atomic ratios in the XPS sampling region were evaluated by peak area integration. The surface morphology and element compositions were examined on a Quanta 200 F scanning electron microscope (SEM) and a Tecnai G2 F20 transmission electron microscope (TEM) (FEI, Hillsboro, OR, USA) with an energy-dispersive X-ray (EDX) spectroscope (FEI, Hillsboro, OR, USA).  $\text{H}_2$ -temperature-programmed reduction ( $\text{H}_2$ -TPR) was performed on an AutoChem II 2920 (Micromeritics, USA) with 10 vol.%  $\text{H}_2$  in Ar. A Magna-IR 560 ESP FT-IR spectrometer (Nicolet, Madison, WI, USA) was used for identifying the functional groups on the surface. The diffuse reflectance spectra were recorded on a U-4100 UV-Vis spectrophotometer (Hitachi, Japan) with an integrated sphere diffuse reflectance attachment. The powder samples were loaded in a transparent quartz cell and UV-Vis absorbance values were measured in the region

of 200–800 nm at room temperature. The reflectance of the standard support was used as the baseline for the relative catalyst measurement.

## Ozonation of Refractory Organic Chemicals

Nitrobenzene is one of typical ROCs in chemically contaminated wastewaters. In the present study, nitrobenzene at a concentration of 100 mg·L<sup>-1</sup> in ultrapure water was used to determine catalytic activity. The initial total organic carbon (TOC) and pH value of nitrobenzene solution were 55 mg·L<sup>-1</sup> and 5.89, respectively.

The COP experiments were performed with a system (Figure S1) that consists of a 40 L of oxygen tank (Beijing Jinggao Gas Co., Ltd., Beijing, China), a COM-AD-02 ozone generator (Anseros Advanced Oxidation Technologies Co., Ltd., Tübingen-Hirschau, Germany), two GM-6000-OEM ozone gas analyzers (Anseros Advanced Oxidation Technologies Co., Ltd., Tübingen-Hirschau, Germany), a D07-7 mass flow controller coupled with a D08-1F flow readout box (Beijing Sevenstar Flow Co., Ltd., Beijing, China), a 800 mL quartz column reactor and an exhaust gas collector. The reactor was placed on a ZNCL-BS intelligent magnetic stirrer (Shanghai Kankun Instrument Equipment Co., Ltd., Shanghai, China) at 700 rpm·min<sup>-1</sup> to promote mass transfer among nitrobenzene, ozone and catalysts. During COP experiments, an aliquot of 500 mL of nitrobenzene solution and 0.5 g of catalyst was added in the reactor at 25°C. The gaseous ozone was then introduced through a porous diffuser at the bottom of the reactor having a flow rate of 7.5 mg·min<sup>-1</sup>. After treatment, nitrogen gas was sparged into the nitrobenzene solution at a rate of 3.0 L·min<sup>-1</sup> to quench the reaction. Fifteen milliliter of treated solution was extracted into a 40 mL of syringe when sampling. The solution in the syringe was then filtered through a 0.45 μm end filter (Tianjin Jinteng Experimental Equipment Co., Ltd., Tianjin, China) to remove catalyst particles before further analysis. The filtered catalyst was dried and recycled for repetitive experiments. The lost amount of the catalyst was supplemented to 0.5 g by addition of the fresh catalyst (~ 5% in average) prior to the next use. After reaction, the concentration of Mn ion in solution was detected by ICP-AES at 259.37 nm for the quantification of Mn. Single adsorption process and single ozonation process (SOP) experiments were performed with the same experimental system as COP. Controls did not have ozone or a catalyst. All adsorption, SOP, and COP experiments were performed in triplicate.

The radicals quenching experiments were performed for identification of the oxidation mechanism. The ·OHs scavenger NaHCO<sub>3</sub> (0.5 and 1.0 g·L<sup>-1</sup>), methanol (5 mg·L<sup>-1</sup>) and the O<sub>2</sub><sup>-</sup> scavenger p-benzoquinone (5 mg·L<sup>-1</sup>) were added into nitrobenzene solution prior to experiments.

Electron spin resonance (ESR) experiments were performed on a Bruker ElexSys E500 spectrometer to directly identify radical species. The test was performed under -183°C (90 K), the operating conditions were centerfield: 3,520 G; sweep width: 200 G; microwave frequency: 9.057 GHz; modulation frequency: 100 GHz; power: 10.00 mW. For radical analysis,

5,5-dimethyl-1-pyrroline (DMPO) was employed as the spin-trapping agents. DMPO was used for capture ·OHs alone, and DMPO with methyl alcohol was used for capture O<sub>2</sub><sup>-</sup>.

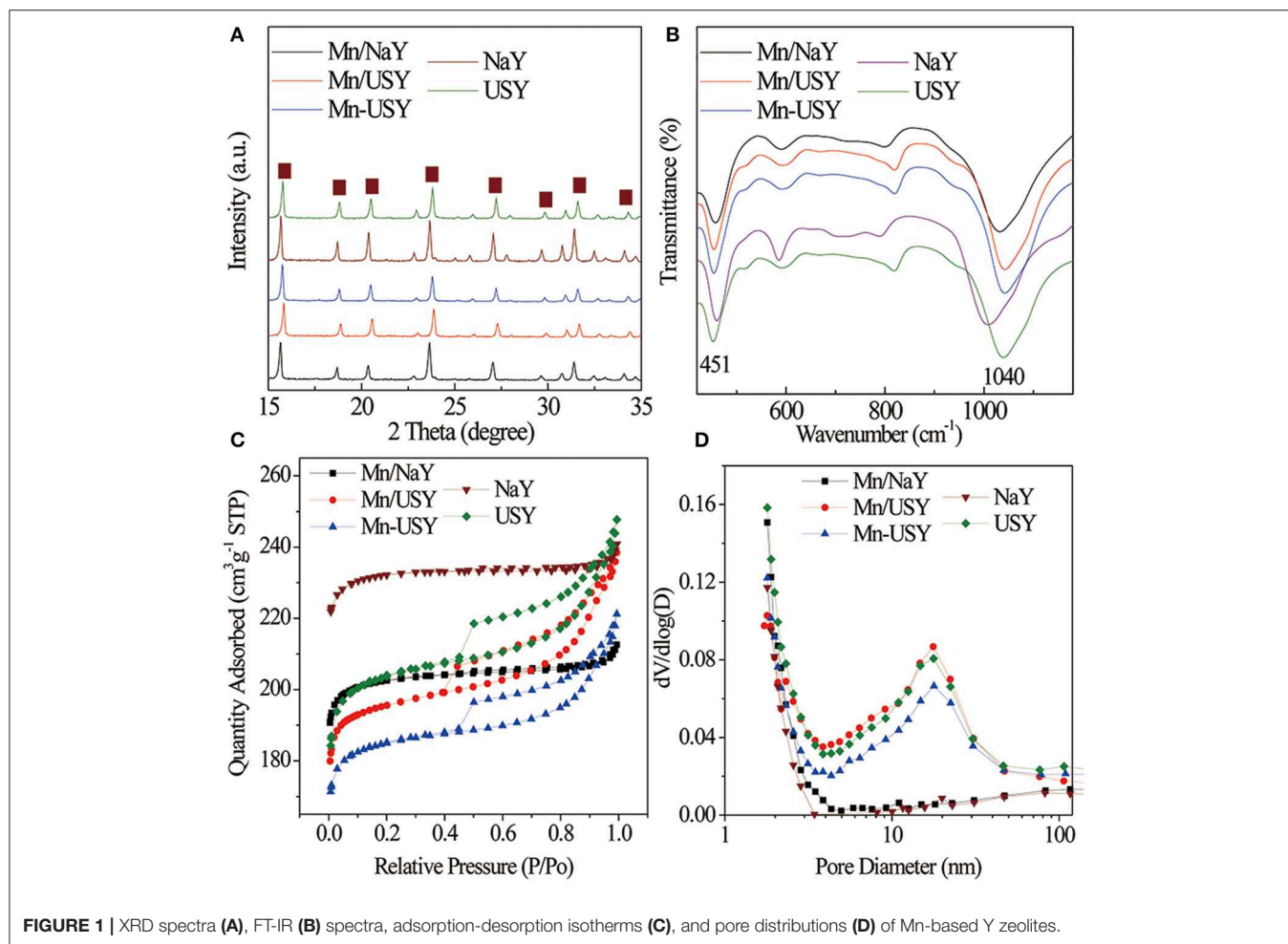
Nitrobenzene and degradation intermediates were identified by a Gas Chromatograph-Mass Spectrometer (GC-MS, 7890 B/MS, Agilent Technologies), a High Performance Liquid Chromatograph (HPLC, Ultimate 3,000, Thermo Scientific) and an Ion Chromatograph (IC, Dionex IC2100, Thermo Scientific). When GC-MS was used for analysis, CH<sub>2</sub>Cl<sub>2</sub> was the extraction solvent. A DB-35 capillary column (30 m × 0.25 mm × 0.25 μm) was used. The initial temperature was 30°C, held for 2 min, increased to 45°C at a rate of 10°C/min and kept for 5 min. It was then heated up to 150°C at a rate of 2°C/min, and kept at 150°C for 5 min, then heated up to 225°C at 2°C/min, and kept at 225°C for 5 min. HPLC was equipped with a Hypersil ODS-C18 column (150 × 4.6 mm × 5 μm), and using a mixture of methanol and ultra-pure water (volume ratio was 4:6) as the mobile phase. The flow rate was 0.8 mL/min. The temperature was maintained at 35°C. The concentration of nitrobenzene and intermediates were detected at 254 and 280 nm, respectively (Zhang and Ma, 2008). Ion chromatographic separation of small organic acids was accomplished on an AG11-HC column (4 × 250 mm). The mobile phase was KOH solution (30 mmol/L). The injection volume was 25 μL. The flow rate was 1.0 mL/min.

## RESULTS AND DISCUSSION

### Characteristics of Catalysts

The XRD peak patterns for both the Y zeolites and Mn-based Y zeolites (Figure 1A) were similar, and have the typical characteristic peaks associated with the FAU type Y zeolite (Li R. et al., 2018). The relative crystallinities were as follows: Mn/NaY (90%), Mn/USY (73%) and Mn-USY (77%), NaY (100%), and USY (81%). Significant crystallinity differences were observed between NaY and USY. Dealumination of the NaY (Si/Al molar ratio at 3.19) results in a partial destruction of the resultant USY (Si/Al, 5.16) skeleton structures, reducing its crystallinity. Introduction of Mn oxides into Y zeolites also results in a slight decrease of relative crystallinity. XRD diffraction peaks from Mn oxides were not observed for the Mn-based Y zeolites, due to surface dispersion, low concentration and/or small size. Negligible but observed changes in the FT-IR spectra of the Y zeolites were noted after loading Mn oxides. A typical peak at about 1,040 cm<sup>-1</sup> (Figure 1B) is attributed to the asymmetrical stretching of Si–O–Si and Al–O–Si bending vibrations in the Y zeolites (Lutz et al., 2010; Asadi et al., 2018). The peak at 451 cm<sup>-1</sup> is related to the Si–O and/or Al–O vibrational bending of the internal tetrahedral aluminosilicate framework (Zhao et al., 2016; Li et al., 2019). The typical absorption peak at 510 cm<sup>-1</sup> due to Mn–O stretching (Naidja et al., 2002) was not observed, due to its masking from the stronger signals produced by the Al–O–Si.

According to IUPAC classification, the adsorption-desorption isotherms of NaY and Mn/NaY exhibited a typical micropore structure (Figure 1C). The isotherms for USY, Mn/USY, and Mn-USY zeolites suggest mixed micropore-mesopore structures due to the partial dealumination of Y zeolites (Denayer and Baron, 1997). The USY, Mn/USY, and Mn-USY had an additional



peak at 20 nm in pore distribution in comparison with NaY and Mn/NaY (Figure 1D). High mesopore areas and pore volumes were observed in USY zeolites relative to NaY zeolites (Table 1). The surface area and pore volume of Y zeolites decrease after loading the Mn oxides because the formed Mn oxides occupy the surface and block the micropores of the Y zeolites (Yang et al., 2019). The differences in surface area and pore volume for the Mn/USY (624 m<sup>2</sup>/g and 0.37 cm<sup>3</sup>/g) and Mn-USY (588 m<sup>2</sup>/g and 0.34 cm<sup>3</sup>/g) are related to the Mn oxides morphology as surface dispersion.

Cubic particles about 400–600 nm were observed on the Y zeolites surface (Figure 2 and Figure S2), which are typical for FAU types of zeolite (Zhang et al., 2019). A microanalysis performed using EDS confirmed the presence of the Mn oxides. Interestingly, the Mn/NaY (Figure 2A), Mn/USY (Figure 2B), and Mn-USY (Figure 2C) varied visually and were dark brown, light brown and blue gray, respectively. The NaY (Figure S2A) and USY (Figure S2B) were white.

The weighted Mn percentages, defined by EDX were: Mn/NaY (5.05%), Mn/USY (3.11%), and Mn-USY (2.75%). The darker colored Mn/NaY is related to the high surface content of the distributed Mn, and the valency of the oxides. The Mn oxides that were deposited on the surfaces of the Y zeolites

formed irregularly shaped micro-agglomerates. The surface Mn oxides were clearly observed according to TEM images of Mn/NaY (Figure 3a) and Mn/USY (Figure 3b) compared to NaY (Figure S3A) and USY (Figure S3B). The Mn oxides on the Mn-USY are unclear in the TEM image (Figure 3c). The USY catalysts exhibit clear mesoporous surface structures by TEM.

The peaks reduced between 200 and 500°C were observed by H<sub>2</sub>-TPR profiles for Mn/NaY, Mn/USY, and Mn-USY (Figure 4A). The Mn/NaY display two well-developed peaks at 200–350 and 350–500°C, while the Mn/USY has a broad undefined peak in 200–500°C. The Mn-USY has a weak peak at 200–350°C and a broad peak at 350–500°C. During the process of hydrogen reduction, the Mn oxides are reduced in two steps: MnO<sub>2</sub> or Mn<sub>2</sub>O<sub>3</sub> → Mn<sub>3</sub>O<sub>4</sub> and Mn<sub>3</sub>O<sub>4</sub> → MnO (Li et al., 2013; Wu et al., 2015). The different multivalent states of Mn oxides coexist with the catalysts. Additionally, the relative peak area at 200–350°C was higher than that at 350–500°C for Mn/NaY, while the opposite trend was observed for Mn-USY. The peak areas for Mn/USY fell between the other two catalysts. Mn having higher valency exists in the Mn/NaY. The reduced peak temperature for the Mn/NaY suggests a weaker interaction between the support and Mn oxides.

**TABLE 1** | Zeolites pore structures determined by N<sub>2</sub> adsorption-desorption and surface element contents by XPS.

Zeolites	NaY	USY	Mn/NaY	Mn/USY	Mn-USY
<b>Pore structures by N<sub>2</sub> adsorption-desorption (surface area: m<sup>2</sup>·g<sup>-1</sup>; pore volume: cm<sup>3</sup>·g<sup>-1</sup>)</b>					
Total surface areas	739	652	646	624	588
Micropore surface areas	706	585	604	565	538
Mesopore surface areas	33	67	42	59	50
Total pore volumes	0.37	0.38	0.33	0.37	0.34
Micropore volumes	0.34	0.28	0.30	0.27	0.26
Mesopore volumes	0.03	0.10	0.03	0.10	0.08
<b>Surface element contents by XPS</b>					
Mn2p weight %			5.03	2.02	1.81
Mn <sup>2+</sup> /Mn <sup>3+</sup> /Mn <sup>4+</sup>			0.20/0.39/0.41	0.33/0.32/0.35	0.43/0.36/0.21

UV-Vis spectra for Mn/NaY, Mn/USY, and Mn-USY were generated between the range of 200–800 nm (**Figure 4B**). The Mn/USY had an absorption at 200–330 (L1) nm and another broad adsorption (L2) between 350 and 650 nm. The absorption profile is associated with a charge transfer (CT) that from O<sup>2-</sup> → Mn<sup>2+</sup> and O<sup>2-</sup> → Mn<sup>4+</sup> and Mn<sup>3+</sup>, respectively (Lamaita et al., 2005; Stamati et al., 2007). The Mn/NaY displayed a weaker L1 and an enhanced L2, while Mn-USY exhibited an enhanced L1 and a weakened L2. This observation suggests a greater Mn<sup>2+</sup> ratio in Mn-USY than that in Mn/NaY and Mn/USY.

XPS was used to further determine Mn distribution and valency. The XPS spectra for Mn/USY and Mn-USY indicate lower content of Na (binding energy at about 1,070 eV) relative to Mn/NaY. This is likely resulted from the removal of Na<sup>+</sup> during NH<sub>4</sub><sup>+</sup> exchange (initial pH value at 3–3.5) for USY preparation (**Figure 5A**). The weight of Na for the Mn/NaY, Mn/USY, and Mn-USY was 7.36, 0.32, and 0.27%, respectively. A strong elemental Mn peak (binding energy at about 640 eV) was observed in Mn/NaY relative to the Mn/USY and Mn-USY, suggesting high surface distribution of Mn oxides. The Mn2p weight was 5.03% for Mn/NaY, 2.02% for Mn/USY, and 1.81% for Mn-USY. The binding energies of Si2p (**Figure 5B**) and Al2p (**Figure 5C**) were at ~101–102 and 72–74 eV, attributable to Si<sup>4+</sup> (Plymale et al., 2015) and Al<sup>3+</sup> (Hadnadjev et al., 2008), respectively. Broad peaks are associated with Al2p XPS for Mn/USY and Mn-USY. The four-coordinate Al framework is partially transformed to five-coordinate Al and non-framework Al during preparation of USY from NaY (Wang et al., 2014). Mn/NaY have low intensity XPS Si2p peaks compared to Mn/USY and Mn-USY, and identical XPS Al2p observed among the catalysts. The surface molar ratio of Si to Al (Si/Al) was 2.7, 4.3, and 3.6 for Mn/NaY, Mn/USY, and Mn-USY, respectively. The observable peak shifts of XPS Si2p and Al2p are related to slight differences in the chemical coordination environment. The XPS spectra from Mn2p are centered between 640–643 and 650–653 eV, and are from the Mn2p<sub>3/2</sub> and Mn2p<sub>1/2</sub> (Zhang

et al., 2015; **Figure 5D**). According to Mn2p<sub>3/2</sub> peaks fitting results, multivalent Mn oxides (Mn<sup>2+</sup>, Mn<sup>3+</sup>, and Mn<sup>4+</sup>) are formed in all the catalysts (Dai et al., 2012). The multivalent Mn in Mn/NaY has the highest Mn<sup>4+</sup> (0.41) content when compared to Mn/USY (0.35) and Mn-USY (0.21). The multivalent Mn in Mn-USY has the highest Mn<sup>2+</sup> (0.43) contents relative to Mn/NaY (0.20) and Mn/USY (0.33). Black or brown coloration is observed for the MnO, MnO<sub>2</sub>, MnOOH, Mn<sub>2</sub>O<sub>3</sub>, and Mn(OH)<sub>2</sub>, a light color is seen with Mn(OH)<sub>2</sub> (white). The valence state (**Figure 5**) and visual color difference (**Figure 2**) suggest that more Mn(OH)<sub>2</sub> (white) is distributed in the Mn-USY catalyst (**Figure 2C**). The different properties for the catalysts observed are resulted from the differences in support material and the methods used to load Mn oxides.

## Catalytic Efficiencies

The adsorption of nitrobenzene in solution quickly reached saturation (4–6%) for all Y zeolites (**Figure 6A**). The Y zeolites exhibited weak adsorption toward nitrobenzene, and slight adsorption capacity differences were observed for the NaY, USY and their Mn-based catalysts. In the previous report using ZSM-5 as catalysts during COP, NaZSM-5 (high Na<sup>+</sup>) had weaker adsorption toward nitrobenzene in solution when compared with HZSM-5 (low Na<sup>+</sup>) (Chen et al., 2018). These results that were influenced by the Na<sup>+</sup> content were not observed with the Y zeolites. The COPs using NaY, USY, Mn/NaY, Mn/USY, and Mn-USY, degraded 31.0, 32.7, 38.8, 44.2, and 49.9% of the nitrobenzene, respectively, 10 min after treatment. In contrary, the SOP degraded 29.5% of the nitrobenzene (**Figure 6B**). Due to catalytic activity of Mn-based Y zeolites, the nitrobenzene degraded after 10 min by COPs was higher than the total sums of SOP and adsorption. Increased activity related with catalysis was however not observed with NaY and USY. The catalytic efficacy between the COPs and SOP gradually decreased with time. After a 60 min treatment, the COPs and SOP degraded identical amounts of nitrobenzene (92–96%).

As determined by TOC, 25.7% of the nitrobenzene was removed after a 60 min treatment using SOP (**Figure 6C**). Including NaY and USY in the COPs reduced TOC by 27.8 and 28.5% of TOC after 60 min treatment. The NaY and USY promote a small increase in TOC that is attributable to the weak adsorption. Using the Mn/NaY, Mn/USY, and Mn-USY as catalysts during COP increases the TOC removal. After a 60 min of treatment, the TOC was reduced by 35.1, 40.0, and 44.3%, respectively. The greater difference in TOC removals cannot be attributed to adsorption (2–4%) (**Figure S4**) and is therefore a realized catalytic influence. The TOC removed by COPs using Mn-based Y zeolites is consistently greater than SOP. The oxidized nitrobenzene produces oxalic acid intermediates (Zhao et al., 2008b) that are further mineralized during COPs with Mn-based Y zeolites, but not with SOP or when NaY and USY are used.

Within 10 min, the pH values of nitrobenzene solution rapidly decreased after the initiation of SOP or COPs, followed by a slow decrease over the treatment time (**Figure 6D**). Higher pH values were observed with the COPs using Mn-based Y zeolites when

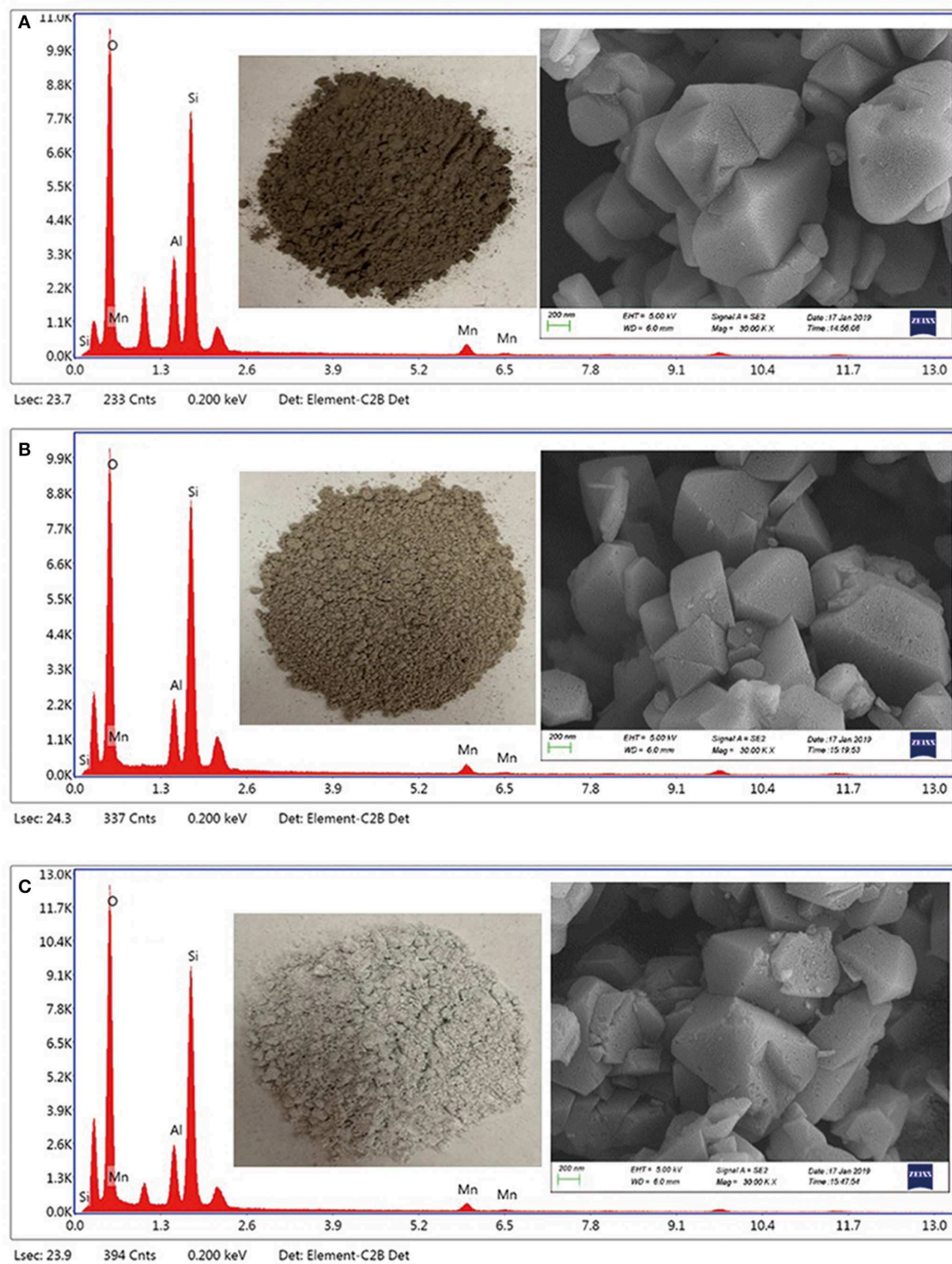
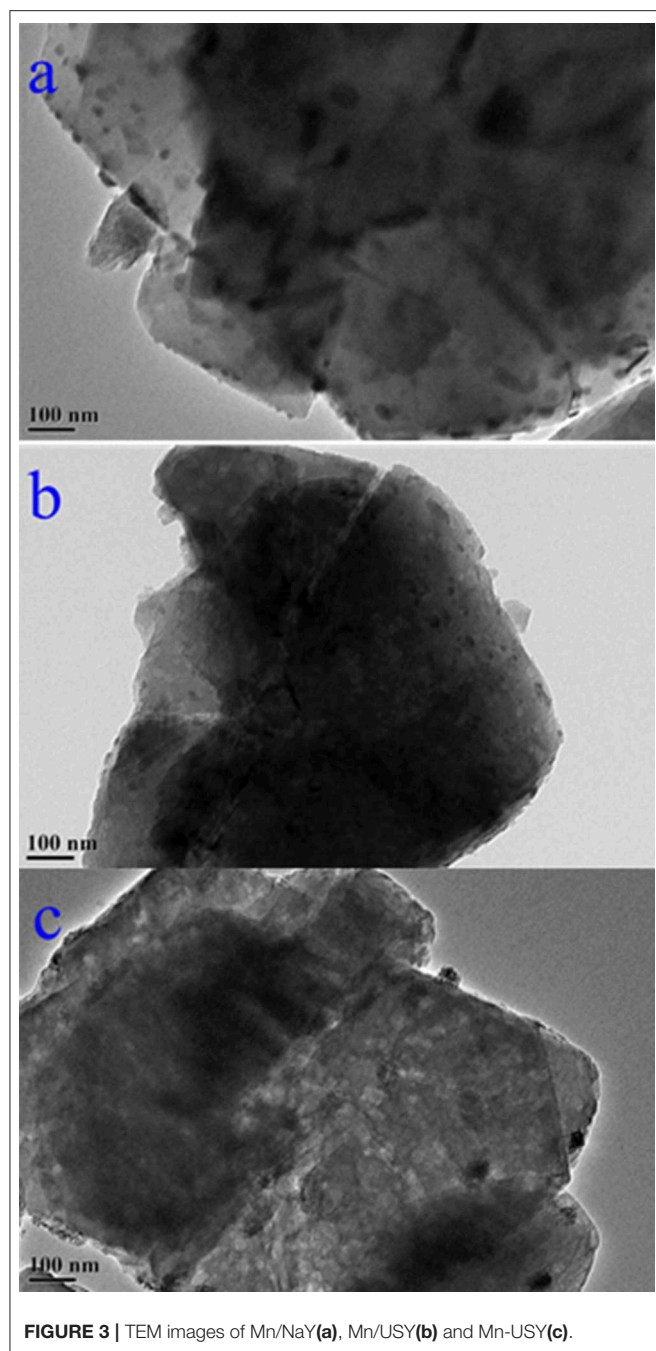


**FIGURE 2 |** SEM images-EDX spectra of Mn/NaY (A), Mn/USY (B), and Mn-USY (C).

compared with COPs containing NaY or USY, and also compared with SOP. Adsorption has little to no influence on pH values. The COPs and SOP generate acidic intermediates that decrease

solution pH values (Zhao et al., 2008a). The Mn-based Y zeolites used during COP further mineralize acidic intermediates, which reduces acidity.



Catalytic activity with the NaY and USY was not observed. The catalytic activities of 4A and ZSM-5 during COP were previously determined (Chen et al., 2018; Ikhlaiq et al., 2018). The types of zeolites and the specific ROCs have an influence on catalytic performances during COPs. The Mn-based Y zeolites are catalytically active, which may be attributed to the multivalent Mn oxides ( $\text{Mn}^{2+}$ ,  $\text{Mn}^{3+}$ , and  $\text{Mn}^{4+}$ ) (Sun et al., 2014; Huang et al., 2017) or the Mn ions in solution (Gracia et al., 1998; Andreozzi et al., 2001). The leaching of Mn ions from catalysts during ozonation was determined by ICP-AES and the concentrations of Mn ions were 4.25, 3.38,

and  $1.75 \text{ mg}\cdot\text{L}^{-1}$  in 60 min of COP with Mn/NaY, Mn/USY and Mn-USY, respectively, after first run. In order to verify the role of Mn ions and Mn oxides in the COP of nitrobenzene, 0.015 g of  $\text{MnO}_x$  and 11  $\mu\text{L}$  of  $\text{Mn}(\text{NO}_3)_2$  solution were added into the ozonation system, respectively. The TOC removal in ozonation of nitrobenzene with  $\text{Mn}^{2+}$  was 28.88% (Figure 6C), slightly higher than single ozonation (25.67%). When NaY and USY were mixed with solid  $\text{MnO}_x$ , both “ $\text{MnO}_x + \text{NaY}$ ” and “ $\text{MnO}_x + \text{USY}$ ” showed approximately 32% of TOC removal in ozonation of nitrobenzene (Figure 6C), which was slightly lower than the COP with Mn/NaY (33.2%). The experimental results suggest that  $\text{MnO}_x$  is the main factor promoting catalytic ozonation of nitrobenzene with Mn-based Y zeolites. The Mn/NaY has relatively low catalytic activity when compared with Mn/USY and Mn-USY. The Mn/NaY did not have high activity during COP, although it had a high concentration of surface distributed Mn. Overly concentrated Mn oxides on the surface can result in aggregation decreasing available active sites (Qi et al., 2012; Chen et al., 2017). It has been previously demonstrated that mesoporous supports can improve the interactions between metallic oxides and facilitate the adsorption of ozone during COPs (Zhuang et al., 2014; Ryu et al., 2019). The mesoporous USY facilitates proximal reactions with the Mn oxides and ozone relative to the microporous NaY. Different methods used for the loading the metal oxides can result in different catalytic performances (Bing et al., 2012). This may plausibly explain why the Mn/USY catalyst exhibits lower catalytic activity in comparison with the Mn-USY catalyst. Additionally, a lower oxide state of Mn facilitates ozone decomposition (Ryu et al., 2019). The highest activity observed for Mn-USY may be also attributed to its high ratio of  $\text{Mn}^{2+}$ .

The leaching of Mn ions (5.83%) from Mn-USY after 60 min reaction was detected by ICP-AES. The reusability of Mn-USY after repeated uses during COP treatment was examined. TOC removal of COP with Mn-USY decreased gradually with the increase of repeated times due to the leaching of Mn from the catalyst. When the number of runs increased from 3 to 4, TOC removals of COP with Mn-USY decreased to <35%, and gradually approaching to the TOC removal in SOP after 5 runs. The results showed Mn-based Y zeolites had a weak-moderate stability in COPs of pollutants, which warrants further investigations to improve the stability of Mn oxides on Y zeolites.

## Mechanisms

The introduction of  $\text{NaHCO}_3$  was performed to confirm whether the generation of  $\cdot\text{OH}$ s promoted the removal of TOC during COP with Mn-USY (Ma and Graham, 2000). Methanol and p-benzoquinone were used to study the roles of the oxygen species in COP with Mn-USY (Khataee et al., 2017; Asgari and Salari, 2019).  $\text{NaHCO}_3$  ( $0.5 \text{ g}\cdot\text{L}^{-1}$ ) significantly reduced the TOC removal during COP with Mn-USY (Figure 7A), which suggests that  $\cdot\text{OH}$  mediates oxidation to remove TOC. When a higher concentration of  $\text{NaHCO}_3$  ( $1.0 \text{ g}\cdot\text{L}^{-1}$ ) was used, changes in TOC removal were not observed, suggesting that the  $\cdot\text{OH}$  generated was mostly consumed. The TOC removal with  $1.0 \text{ g}\cdot\text{L}^{-1}$  of  $\text{NaHCO}_3$  in the COP using the Mn-USY was higher than by SOP. The other active oxygen species (other than  $\cdot\text{OH}$ s) coexist during

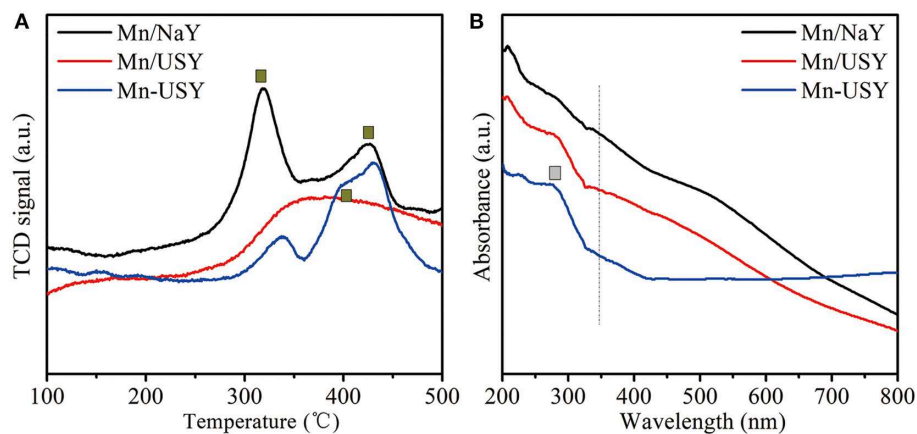


FIGURE 4 | H<sub>2</sub>-TPR (A) and UV-vis (B) spectra of Mn/NaY, Mn/USY, and Mn-USY.

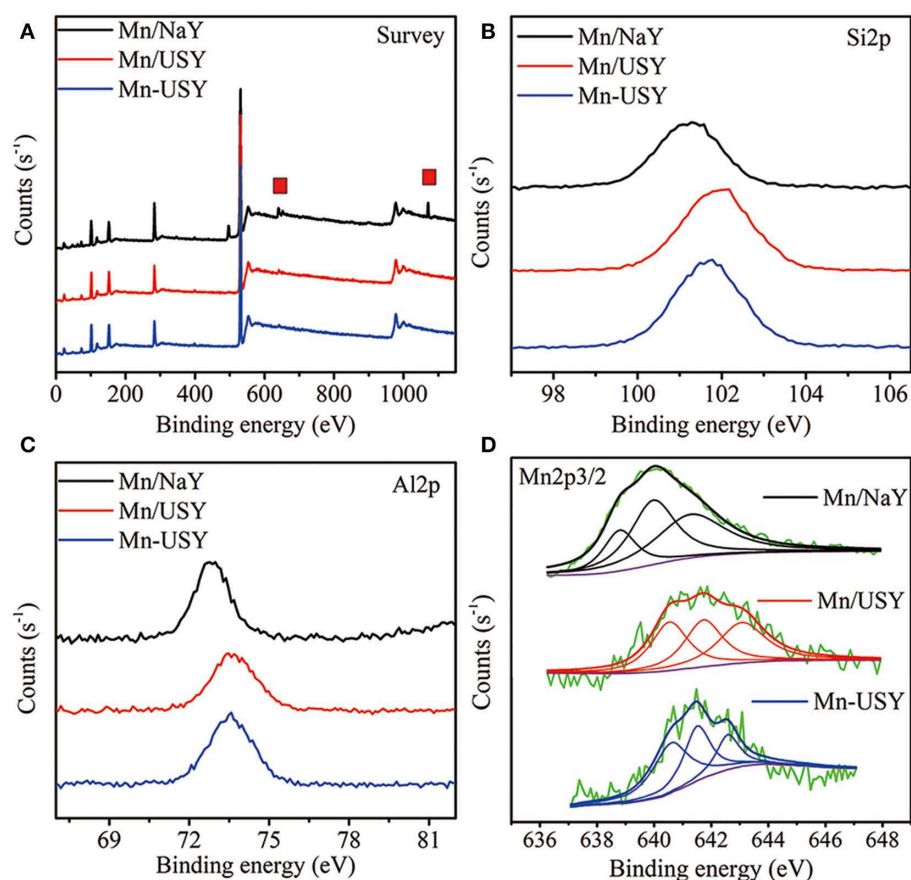
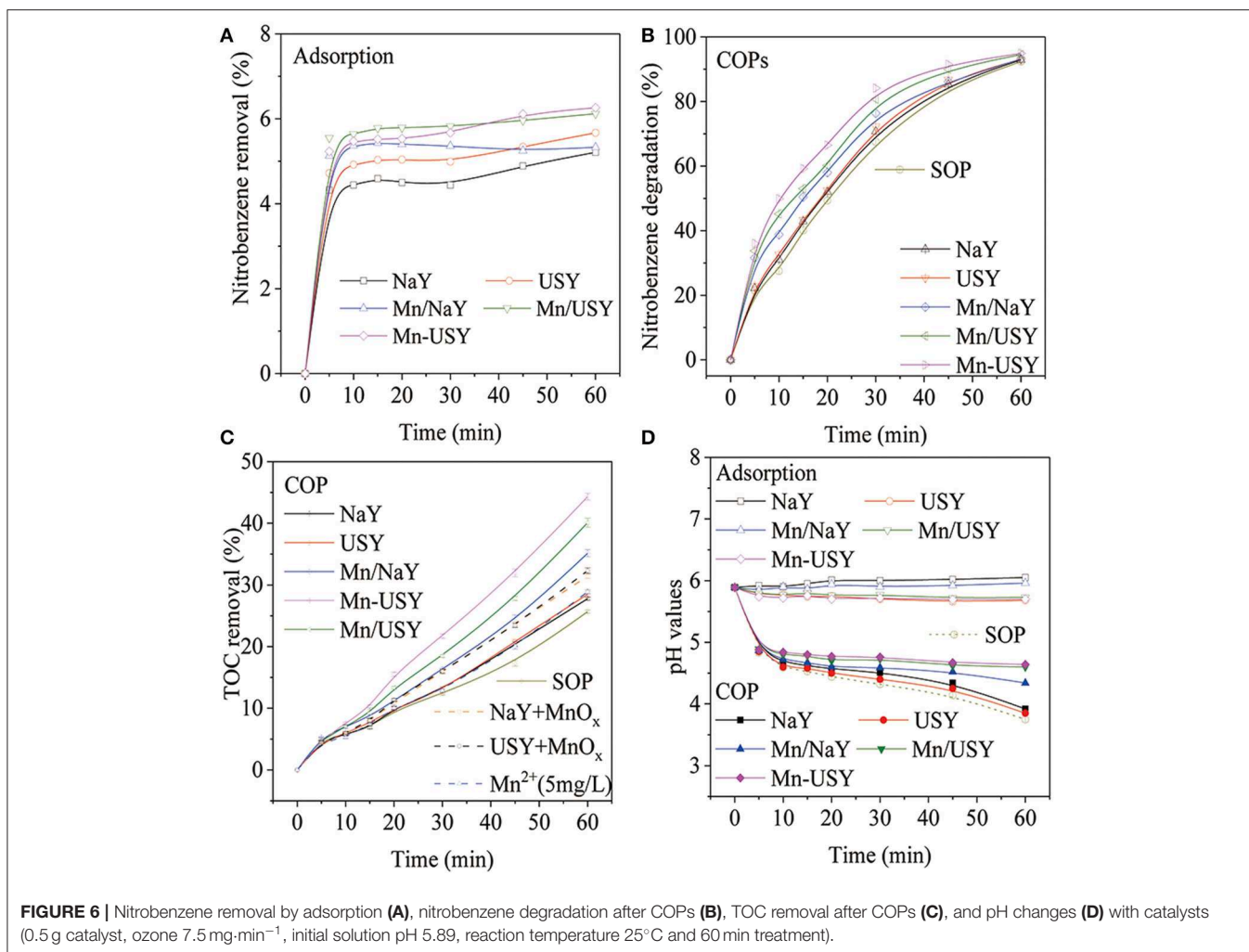


FIGURE 5 | Survey (A), Si2p (B), Al2p (C) and Mn2p (D) XPS spectra of Mn/NaY, Mn/USY and Mn-USY.

COP. This contributes toward the mineralization of nitrobenzene in solution. The degradation of nitrobenzene significantly decreased to 77.5% upon addition of methanol ( $5 \text{ mg}\cdot\text{L}^{-1}$ ) (Figure 7B). After addition of both methanol ( $5 \text{ mg}\cdot\text{L}^{-1}$ ) and p-benzoquinone ( $5 \text{ mg}\cdot\text{L}^{-1}$ ), the degradation of nitrobenzene

dropped to 72.4% at 30 min. The experimental results showed that  $\cdot\text{OH}$ s and  $\text{O}_2^{\cdot-}$  promote the degradation of nitrobenzene. ESR was performed to directly detect the radicals and it does prove this. The DMPO- $\cdot\text{OH}$  peak (Figure 7C) has an intensity ratio of 1:2:2:1 (Fang et al., 2009) and DMPO- $\text{O}_2^{\cdot-}$  (Figure 7D)



is peaked at 1:1:1:1 (Zhao et al., 2018), further confirming the production of  $\cdot\text{OH}$  and  $\text{O}_2^{\cdot-}$  during COP with Mn-USY. The multivalent Mn oxides ( $\text{Mn}^{2+}$ ,  $\text{Mn}^{3+}$ , and  $\text{Mn}^{4+}$ ) in Mn-USY promotes the generation of  $\cdot\text{OH}$ s and  $\text{O}_2^{\cdot-}$  by the transferring electrons between the metallic oxides and ozone molecules.

## Proposed Pathways for Nitrobenzene Degradation

In order to better understand the pathways of nitrobenzene degradation during COP, the intermediates formed during the degradation of nitrobenzene by COP using Mn-USY were determined by GC-MS, HPLC, and IC. Figure 8 shows that p-nitrophenol, m-nitrophenol, o-nitrophenol, phenol, resorcinol, hydroquinone, catechol, p-benzoquinone, 4-nitrocatechol, 1, 3, 4-trihydroxy-6-nitrobenzene, nitrate, carbonate, oxalic acid, formic acid, acetic acid, succinic acid, maleic acid, and fumaric acid were generated during COP. The production of phenol indicated the occurrence of denitration. The nitro group can be removed from nitrobenzene by a nucleophilic substitution reaction with ozone and  $\text{O}_2^{\cdot-}$ , and the unstable intermediates were then further oxidized to phenol (Wang et al., 2015; Yang et al., 2018). Alternatively, the  $\cdot\text{OH}$ s can transfer electron forming

phenyl radicals that can be in turn transformed into phenol (Zhao et al., 2008a). The phenolic hydroxyl group belongs to the electron-donating group, ozone molecules and  $\cdot\text{OH}$ s tend to react with the ortho- and para-positions of hydroxyl to form catechol and hydroquinone. With further oxidation, p-benzoquinone and 1, 2, 4-trihydroxybenzene are formed prior to ring opening. The accumulation of p-benzoquinone concentration increases to its maximum after 20 min, confirming this.

Moreover,  $\cdot\text{OH}$ s could easily react with the  $\alpha$ -,  $\beta$ -, or/and  $\gamma$ -carbons of nitrobenzene by electrophilic addition to form o-nitrophenol, m-nitrophenol, and p-nitrophenol, respectively (Bhatkhande et al., 2003). During the COP, the concentration of p-nitrophenol, m-nitrophenol and o-nitrophenol is low, indicating that the electrophilic radicals may continue to attack p-nitrophenol, m-nitrophenol and o-nitrophenol. Similarly, the reaction can occur preferentially in the ortho- and para- positions of phenolic hydroxyl groups (Goi et al., 2004). The  $\cdot\text{OH}$ s attack the carbon atoms attached to the nitro group and nitrate ions are released by the radical addition. The  $\cdot\text{OH}$ s electrophilic addition occurs continuously to form resorcinol, hydroquinone, catechol, 4-nitrocatechol and 1,3,4-trihydroxy-6-nitrobenzene.

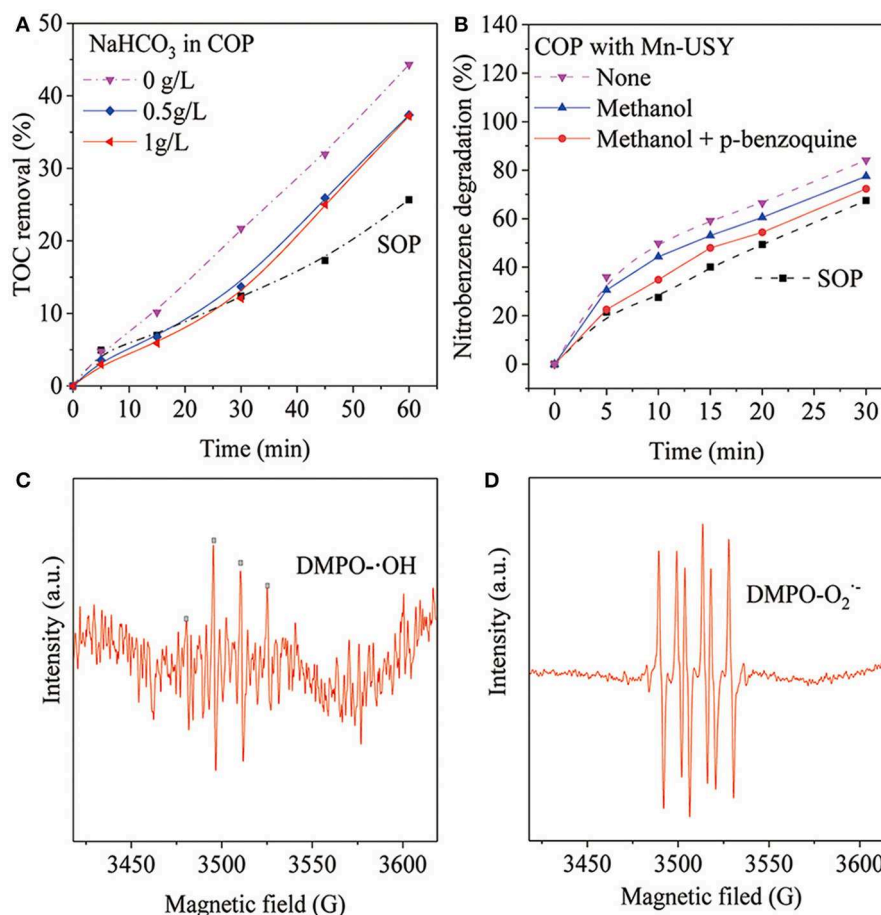


**FIGURE 7** | TOC reduction after COP treatment (60 min) using Mn-USY with the addition of NaHCO<sub>3</sub> (A), methanol (5 mg·L<sup>-1</sup>) and p-benzoquinone (5 mg·L<sup>-1</sup>) (B), liquid-phase ESR spectra of ·OHs (C) and O<sub>2</sub><sup>-</sup> (D) with DMPO spin trapping.

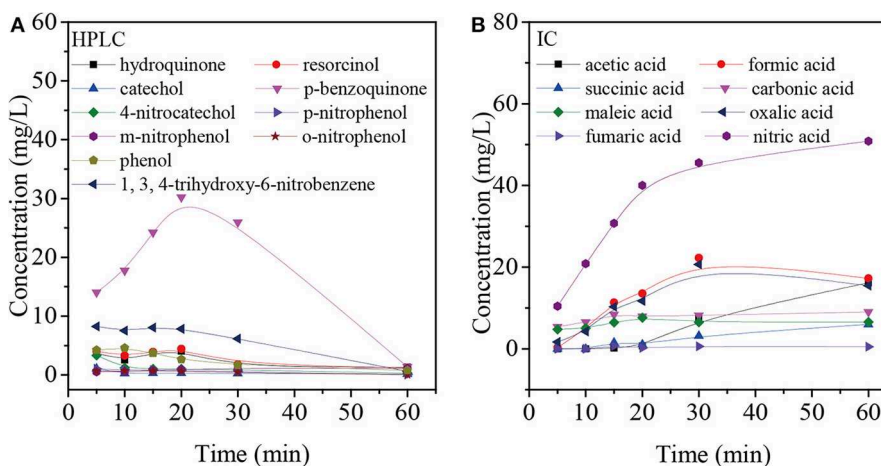
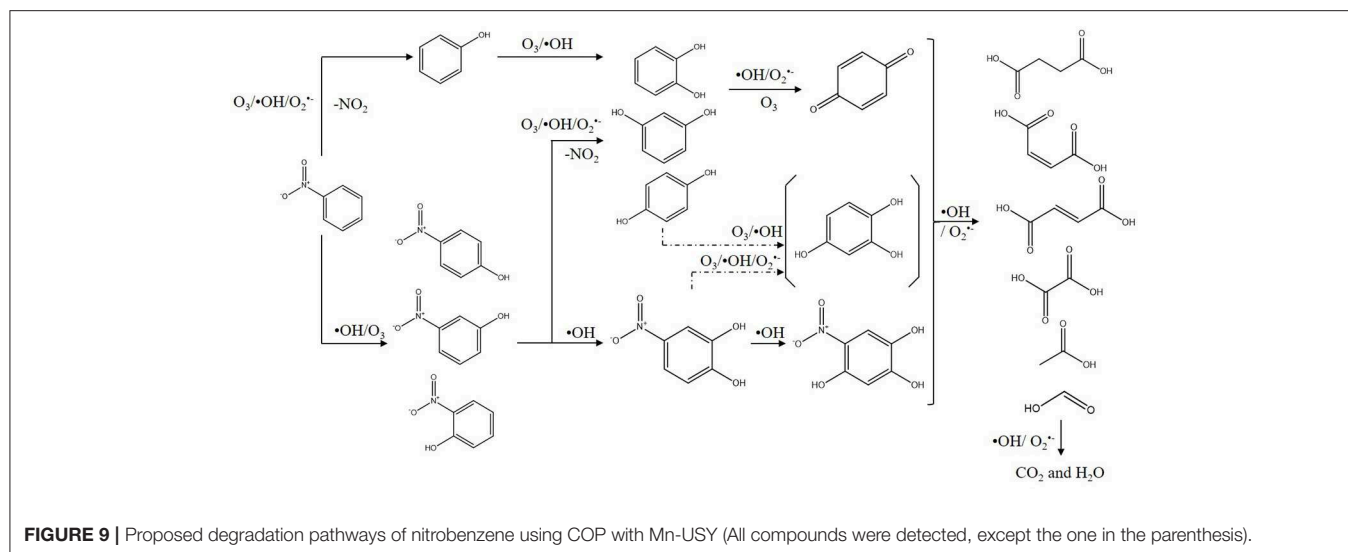


**FIGURE 8** | Intermediate products based on HPLC (A) and IC (B) from the degradation of nitrobenzene using COP with Mn-USY.

The above-mentioned intermediates will further react with ·OHs forming carboxylic acid such as formic acid, acetic acid and oxalic acid. These small molecules are finally mineralized

to CO<sub>2</sub> and H<sub>2</sub>O. In addition, the accumulation of nitrate indicates that the COP has been accompanied by the reaction of denitration (Figure 9).



## CONCLUSIONS

The catalysts of Mn-based Y zeolites were investigated for catalytic ozonation efficiencies and mechanisms during the COP treatment of nitrobenzene in water. The multivalent Mn oxides ( $Mn^{2+}$ ,  $Mn^{3+}$ , and  $Mn^{4+}$ ) are highly dispersed on the surface of NaY or USY, and function as catalytically active sites that increase mineralization. The Mn-USY removed the most TOC during COP which is related to its high surface ratio of  $Mn^{2+}$ , and coordinated interaction between the Mn oxides and mesoporous structures. The oxidation is mediated by  $\cdot OH$ s and  $O_2^{\cdot -}$ , contributing to the TOC removal. These catalytic mechanistic results are broadly applicable to catalyst design for use with the COP treatment of ROCs in water.

## DATA AVAILABILITY STATEMENT

The datasets generated for this study are available on request to the corresponding author.

## AUTHOR CONTRIBUTIONS

JH and CC conceived and designed the experiments. JH, SN, and YimL performed the experiments. JH, YZ, QW, BY, and

SG interpreted and analyzed the data. YifL and SN contributed reagents, materials, analysis tools. BY, QL, CC, and JH. wrote the manuscript.

## FUNDING

This study was supported in part by the National Natural Science Foundation of China (No. 21776307) and the Independent Project Program of State Key Laboratory of Petroleum Pollution Control (Grant No. PPCIP2017004), CNPC Research Institute of Safety and Environmental Technology.

## SUPPLEMENTARY MATERIAL

The Supplementary Material for this article can be found online at: <https://www.frontiersin.org/articles/10.3389/fchem.2020.00080/full#supplementary-material>

**Figure S1** | Schematic representation of the experimental setup.

**Figure S2** | SEM images and EDX spectra of NaY (a) and USY (b).

**Figure S3** | TEM images of NaY (a) and USY (b).

**Figure S4** | TOC removal in adsorption process with Y zeolites.

## REFERENCES

- Andreozzi, R., Caprio, V., Marotta, R., and Tufano, V. (2001). Kinetic modeling of pyruvic acid ozonation in aqueous solutions catalyzed by Mn(II) and Mn(IV) ions. *Water Res.* 35, 109–120. doi: 10.1016/S0043-1354(00)00237-2
- Asadi, A. A., Alavi, S. M., Royaei, S. J., and Bazmi, B. (2018). Dependency of acidic and surficial characteristics of steamed Y zeolite on potentially effective synthesis parameters: screening, prioritizing and model development. *Micropor. Mesopor. Mat.* 259, 142–154. doi: 10.1016/j.micromeso.2017.09.028
- Asgari, G., and Salari, M. (2019). Optimized synthesis of carbon-doped nano-MgO and its performance study in catalyzed ozonation of humic acid in aqueous

- solutions: modeling based on response surface methodology. *J. Environ. Manage.* 239, 198–210. doi: 10.1016/j.jenvman.2019.03.055
- Bhatkhande, D. S., Pangarkar, V. G., and Beenackers, A. A. C. M. (2003). Photocatalytic degradation of nitrobenzene using titanium dioxide and concentrated solar radiation: chemical effects and scaleup. *Water Res.* 37, 1223–121230. doi: 10.1016/S0043-1354(02)00490-6
- Bing, J., Li, L., Lan, B., Liao, G., Zeng, J., Zhang, Q., et al. (2012). Synthesis of cerium-doped MCM-41 for ozonation of p-chlorobenzoic acid in aqueous solution. *Appl Catal B Environ.* 115–6, 16–24. doi: 10.1016/j.apcatb.2011.12.017
- Chen, C., Ma, W., Guo, S., Wang, Q., and Li, Q. X. (2017). Mn-Fe-Mg-Ce loaded Al<sub>2</sub>O<sub>3</sub> catalyzed ozonation for mineralization of refractory organic

- chemicals in petroleum refinery wastewater. *Sep. Purif. Technol.* 183, 1–10. doi: 10.1016/j.seppur.2017.03.054
- Chen, C., Yan, X., Xu, Y., Yoza, B. A., Wang, X., Kou, Y., et al. (2019). Activated petroleum waste sludge biochar for efficient catalytic ozonation of refinery wastewater. *Sci. Total Environ.* 651, 2631–2640. doi: 10.1016/j.scitotenv.2018.10.131
- Chen, C., Yan, X., Yoza, B. A., Zhou, T., Li, Y., Zhan, Y., et al. (2018). Efficiencies and mechanisms of ZSM-5 zeolites loaded with cerium, iron, or manganese oxides for catalytic ozonation of nitrobenzene in water. *Sci. Total Environ.* 612, 1424–1432. doi: 10.1016/j.scitotenv.2017.09.019
- Chen, C., Yoza, B. A., Chen, H., and Li, Q. X. (2015). Manganese sand ore is an economical and effective catalyst for ozonation of organic contaminants in petrochemical wastewater. *Water Air Soil Pollut.* 226:182. doi: 10.1007/s11270-015-2446-y
- Dai, Y., Wang, X., Dai, Q., and Li, D. (2012). Effect of Ce and La on the structure and activity of MnOx catalyst in catalytic combustion of chlorobenzene. *Appl. Catal. B Environ.* 111–112, 141–149. doi: 10.1016/j.apcatb.2011.09.028
- Dasgupta, A., Matos, J., Muramatsu, H., Ono, Y., Gonzalez, V., Liu, H., et al. (2018). Nanostructured carbon materials for enhanced nitrobenzene adsorption: physical vs. chemical surface properties. *Carbon* 139, 833–844. doi: 10.1016/j.carbon.2018.07.045
- Denayer, J., and Baron, G. (1997). Adsorption of normal and branched paraffins in faujasite zeolites NaY, HY, Pt/Nay and USY. *Adsorption* 3, 251–265. doi: 10.1007/BF01653628
- Dong, Y., Yang, H., He, K., Wu, X., and Zhang, A. (2008). Catalytic activity and stability of  $\gamma$  zeolite for phenol degradation in the presence of ozone. *Appl. Catal. B Environ.* 82, 163–168. doi: 10.1016/j.apcatb.2008.01.023
- Einaga, H., Teraoka, Y., and Ogat, A. (2011). Benzene oxidation with ozone over manganese oxide supported on zeolite catalysts. *Catal. Today* 164, 571–574. doi: 10.1016/j.cattod.2010.10.067
- El Metwally, A. E., Eshaq, G., Al-Sabagh, A. M., Yehia, F. Z., Philip, C. A., Moussa, N. A., et al. (2019). Insight into heterogeneous fenton-sonophotocatalytic degradation of nitrobenzene using metal oxochlorides. *Sep. Purif. Technol.* 210, 452–462. doi: 10.1016/j.seppur.2018.08.029
- Fang, Y., Deng, A., and Huang, Y. (2009). Determination of hydroxyl radical in fenton system. *Chin. Chem. Lett.* 20, 1235–121240. doi: 10.1016/j.ccllet.2009.05.004
- Goi, A., Trapido, M., and Tuhkanen, T. (2004). A study of toxicity, biodegradability, and some by-products of ozonised nitrophenols. *Adv. Environ. Res.* 8, 303–3311. doi: 10.1016/S1093-0191(02)00102-8
- Gracia, R., Aragües, J. L., and Ovelheiro, J. L. (1998). Mn(II)-catalyzed ozonation of raw ebro river water and its ozonation by products. *Water Res.* 32, 57–62. doi: 10.1016/S0043-1354(97)00188-7
- Hadnadjev, M., Vulic, T., and Marinkovic-Neducin, R. (2008). The iron oxidation state in Mg-Al-Fe mixed oxides derived from layered double hydroxides: an XPS study. *Appl. Surf. Sci.* 254, 4297–4302. doi: 10.1016/j.apsusc.2008.01.063
- Huang, Y., Sun, Y., Xu, Z., Luo, M., Zhu, C., and Li, L. (2017). Removal of aqueous oxalic acid by heterogeneous catalytic ozonation with MnOx/sewage sludge-derived activated carbon as catalysts. *Sci. Total Environ.* 575, 50–57. doi: 10.1016/j.scitotenv.2016.10.026
- Ikhlaq, A., Brown, D. R., and Kasprzyk-Hordern, B. (2013). Mechanisms of catalytic ozonation: an investigation into superoxide ion radical and hydrogen peroxide formation during catalytic ozonation on alumina and zeolites in water. *Appl. Catal. B Environ.* 129, 437–449. doi: 10.1016/j.apcatb.2012.09.038
- Ikhlaq, A., Waheed, S., Joya, K. S., and Kazmi, M. (2018). Catalytic ozonation of paracetamol on zeolite a: non-radical mechanism. *Catal. Commun.* 12, 15–20. doi: 10.1016/j.catcom.2018.01.010
- Jeirani, Z., and Soltan, J. (2017). Improved formulation of Fe-MCM-41 for catalytic ozonation of aqueous oxalic acid. *Chem. Eng. J.* 307, 756–765. doi: 10.1016/j.cej.2016.08.141
- Khataee, A., Rad, T. S., and Fathinia, M. (2017). The role of clinoptilolite nanosheets in catalytic ozonation process: insights into the degradation mechanism, kinetics and the toxicity. *J. Taiwan Inst. Chem. Eng.* 77, 205–2215. doi: 10.1016/j.jtice.2017.05.004
- Kwong, C., Chao, C. Y. H., Hui, K. S., and Wan, M. P. (2008). Catalytic ozonation of toluene using zeolite and MCM-41 materials. *Environ. Sci. Technol.* 42, 8504–8509. doi: 10.1021/es801087f
- Lamaita, L., Peluso, M. A., Sambeth, J. E., and Thomas, H. J. (2005). Synthesis and characterization of manganese oxides employed in VOCs abatement. *Appl. Catal. B Environ.* 61, 114–119. doi: 10.1016/j.apcatb.2005.03.014
- Li, J., Li, L., Wu, F., Zhang, L., and Liu, X. (2013). Dispersion-precipitation synthesis of nanorod Mn<sub>3</sub>O<sub>4</sub> with high reducibility and the catalytic complete oxidation of air pollutants. *Catal. Commun.* 31, 52–56. doi: 10.1016/j.catcom.2012.11.013
- Li, R., Chong, S., Altaf, N., Gao, Y., Louis, B., and Wang, Q. (2019). Synthesis of ZSM-5/siliceous zeolite composites for improvement of hydrophobic adsorption of volatile organic compounds. *Front. Chem.* 7:505. doi: 10.3389/fchem.2019.00505
- Li, R., Xue, T., Bingre, R., Gao, Y., Louis, B., and Wang, Q. (2018). Microporous zeolite@vertically aligned Mg-Al layered double hydroxide core@shell structures with improved hydrophobicity and toluene adsorption capacity under wet conditions. *ACS Appl. Mater. Interf.* 10, 34834–34839. doi: 10.1021/acsami.8b15118
- Li, Y., Wei, G., He, H., Liang, X., Chu, W., Huang, D., et al. (2018). Improvement of zinc substitution in the reactivity of magnetite coupled with aqueous Fe(II) towards nitrobenzene reduction. *Colloid Interface Sci.* 517, 104–112. doi: 10.1016/j.jcis.2018.01.103
- Lutz, W., Kurzhals, R., Kryukova, G., Enke, D., Weber, M., and Heidemann, D. (2010). Formation of mesopores in USY zeolites: a case revisited. *Z. Anorg. Allg. Chem.* 636, 1497–1505. doi: 10.1002/zaac.201000025
- Ma, J., and Graham, N. J. D. (2000). Degradation of atrazine by manganese-catalysed ozonation—influence of radical scavengers. *Water Res.* 34, 3822–3823828. doi: 10.1016/S0043-1354(00)00130-5
- Naidja, A., Liu, C., and Huang, P. M. (2002). Formation of protein-birnessite complex: XRD, FTIR, and AFM analysis. *J. Colloid Interf. Sci.* 251, 46–56. doi: 10.1006/jcis.2002.8349
- Nawrocki, J., and Kasprzyk-Hordern, B. (2010). The efficiency and mechanisms of catalytic ozonation. *Appl. Catal. B Environ.* 99, 27–42. doi: 10.1016/j.apcatb.2010.06.033
- Plymale, N. T., Kim, Y. G., Soriaga, M. P., and Brunschwigg, B. S. (2015). Synthesis, characterization, and reactivity of ethynyl- and propynyl-terminated Si (111) surfaces. *J. Phys. Chem. C* 119, 19847–19862. doi: 10.1021/acs.jpcc.5b05028
- Qi, F., Xu, B., Zhao, L., Chen, Z., Zhang, L., Sun, D., et al. (2012). Comparison of the efficiency and mechanism of catalytic ozonation of 2, 4, 6-trichloroanisole by iron and manganese modified bauxite. *Appl. Catal. B Environ.* 121–2, 171–81. doi: 10.1016/j.apcatb.2012.04.003
- Rosal, R., Gonzalo, M., Rodríguez, A., Perdígón-Melón, J., and García-Calvo, E. (2010). Catalytic ozonation of atrazine and linuron on MnOx/Al<sub>2</sub>O<sub>3</sub> and MnOx/SBA-15 in a fixed bed reactor. *Chem. Eng. J.* 165, 806–812. doi: 10.1016/j.cej.2010.10.020
- Ryu, H. W., Song, Y., Park, J. S., Kim, J. M., Jung, S. C., Song, J., et al. (2019). Removal of toluene using ozone at room temperature over mesoporous Mn/Al<sub>2</sub>O<sub>3</sub> catalysts. *Environ. Res.* 172, 649–657. doi: 10.1016/j.envres.2019.03.016
- Santikunaporn, M., Herrera, J. E., Jongpatiwut, S., Resasco, D. E., Alvarez, W. E., and Sughrue, E. L. (2004). Ring opening of decalin and tetralin on HY and Pt/HY zeolite catalysts. *J. Catal.* 228, 100–113. doi: 10.1016/j.jcat.2004.08.030
- Sato, K., Iwata, Y., Miki, Y., and Shimada, H. (1999). Hydrocracking of tetralin over NiW/USY zeolite catalysts: for the improvement of heavy-oil upgrading catalysts. *J. Catal.* 186, 45–56. doi: 10.1006/jcat.1999.2546
- Sato, K., Nishimura, Y., Honna, K., Matsubayashi, N., and Shimada, H. (2001). Role of HY zeolite mesopores in hydrocracking of heavy oils. *J. Catal.* 200, 288–297. doi: 10.1006/jcat.2001.3184
- Stamati, N., Goundani, K., Vakros, J., Bourikas, K., and Kordulis, C. (2007). Influence of composition and preparation method on the activity of MnOx/Al<sub>2</sub>O<sub>3</sub> catalysts for the reduction of benzaldehyde with ethanol. *Appl. Catal. A Gen.* 325, 322–327. doi: 10.1016/j.apcata.2007.02.044
- Sui, M., Liu, J., and Li, S. (2011). Mesoporous material supported manganese oxides (MnOx/MCM-41) catalytic ozonation of nitrobenzene in water. *Appl. Catal. B Environ.* 106, 195–203. doi: 10.1016/j.apcatb.2011.05.025
- Sun, Q., Li, L., Yan, H., Hong, X., Hui, K. S., and Pan, Z. (2014). Influence of the surface hydroxyl groups of MnOx/SBA-15 on heterogeneous catalytic ozonation of oxalic acid. *Chem. Eng. J.* 242, 348–356. doi: 10.1016/j.cej.2013.12.097

- Valdes, H., Tardon, R. F., and Zaror, C. A. (2012). Role of surface hydroxyl groups of acid-treated natural zeolite on the heterogeneous catalytic ozonation of methylene blue contaminated waters. *Chem. Eng. J.* 211–2, 388–95. doi: 10.1016/j.cej.2012.09.069
- Vu, H., Harth, F. M., and Wilde, N. (2018). Silylated zeolites with enhanced hydrothermal stability for the aqueous-phase hydrogenation of levulinic acid to gamma-valerolactone. *Front. Chem.* 6:143. doi: 10.3389/fchem.2018.00143
- Wang, F., and Ma, Y. (2018). MPC-973: a low-cost and effective adsorbent for the removal of nitrobenzene from aqueous solutions. *Mater. Chem. Phys.* 208, 157–162. doi: 10.1016/j.matchemphys.2018.01.049
- Wang, X., Deng, X., Bai, Z., Zhang, X., Feng, X., and Huang, W. (2014). The synthesis of super-hydrophilic and acid-proof Ge-ZSM-5 membranes by simultaneous incorporation of Ge and Al into a silicalite-1 framework. *J. Membr. Sci.* 468, 202–208. doi: 10.1016/j.memsci.2014.06.007
- Wang, Y., Cao, H., Chen, C., Xie, Y., Sun, H., Duan, X., et al. (2019). Metal-free catalytic ozonation on surface-engineered graphene: microwave reduction and heteroatom doping. *Chem. Eng. J.* 355, 118–129. doi: 10.1016/j.cej.2018.08.134
- Wang, Y., Xie, Y., Sun, H., Xiao, J., Cao, H., and Wang, S. (2015). Hierarchically shape-controlled mixed-valence calcium manganites for catalytic ozonation of aqueous phenolic compounds. *Catal. Sci. Technol.* 6, 2918–2929. doi: 10.1039/C5CY01967B
- Wu, G., Gao, Y., Ma, F., Zheng, B., Liu, L., Sun, H., et al. (2015). Catalytic oxidation of benzyl alcohol over manganese oxide supported on MCM-41 zeolite. *Chem. Eng. J.* 271, 14–22. doi: 10.1016/j.cej.2015.01.119
- Xu, Y., Wang, Q., Yoza, B. A., Li, Q. X., Kou, Y., Tang, Y., et al. (2019). Catalytic ozonation of recalcitrant organic chemicals in water using vanadium oxides loaded ZSM-5 zeolites. *Front. Chem.* 7:384. doi: 10.3389/fchem.2019.00384
- Yan, H., Chen, W., Liao, G., Li, X., Ma, S., and Li, L. (2016). Activity assessment of direct synthesized Fe-SBA-15 for catalytic ozonation of oxalic acid. *Sep. Purif. Technol.* 159, 1–6. doi: 10.1016/j.seppur.2015.12.055
- Yang, P., Luo, S., Liu, Y., and Jiao, W. (2018). Degradation of nitrobenzene wastewater in an acidic environment by Ti(IV)/H<sub>2</sub>O<sub>2</sub>/O<sub>3</sub> in a rotating packed bed. *Environ. Sci. Pollut. Res.* 25, 25060–25070. doi: 10.1007/s11356-018-2551-8
- Yang, X., Cheng, X., Elzatahry, A. A., Chen, J., Alghamdi, A., and Deng, Y. (2019). Recyclable fenton-like catalyst based on zeolite Y supported ultrafine, highly-dispersed Fe<sub>2</sub>O<sub>3</sub> nanoparticles for removal of organics under mild conditions. *Chin. Chem. Lett.* 30, 324–330. doi: 10.1016/j.ccl.2018.06.026
- Zhang, R., Xu, S., Raja, D., Khusni, N. B., Liu, J., Zhang, J., et al. (2019). On the effect of mesoporosity of FAU Y zeolites in the liquid-phase catalysis. *Micr. Meso. Mater.* 278, 297–306. doi: 10.1016/j.micromeso.2018.12.003
- Zhang, T., and Ma, J. (2008). Catalytic ozonation of trace nitrobenzene in water with synthetic goethite. *J. Mol. Catal. A Chem.* 279, 82–89. doi: 10.1016/j.molcata.2007.09.030
- Zhang, Z., Liu, B., Wang, F., and Zheng, S. (2015). High-temperature desulfurization of hot coal gas on Mo modified Mn/KIT-1 sorbents. *Chem. Eng. J.* 272, 69–78. doi: 10.1016/j.cej.2015.02.091
- Zhao, J., Yin, Y., Li, Y., Chen, W., and Liu, B. (2016). Synthesis and characterization of mesoporous zeolite  $\gamma$  by using block copolymers as templates. *Chem. Eng. J.* 284, 405–411. doi: 10.1016/j.cej.2015.08.143
- Zhao, J., Zhao, Z., Li, N., Nan, J., Yu, R., and Du, J. (2018). Visible-light-driven photocatalytic degradation of ciprofloxacin by a ternary Mn<sub>2</sub>O<sub>3</sub>/Mn<sub>3</sub>O<sub>4</sub>/MnO<sub>2</sub> valence state heterojunction. *Chem. Eng. J.* 353, 805–8813. doi: 10.1016/j.cej.2018.07.163
- Zhao, L., Ma, J., and Sun, Z. (2008a). Oxidation products and pathway of ceramic honeycomb-catalyzed ozonation for the degradation of nitrobenzene in aqueous solution. *Appl. Catal. B Environ.* 79, 244–253. doi: 10.1016/j.apcatb.2007.10.026
- Zhao, L., Ma, J., Sun, Z., and Zhai, X. (2008b). Catalytic ozonation for the degradation of nitrobenzene in aqueous solution by ceramic honeycomb-supported manganese. *Appl. Catal. B Environ.* 83, 256–264. doi: 10.1016/j.apcatb.2008.02.009
- Zhao, L., Sun, Z., Ma, J., and Liu, H. (2009). Enhancement mechanism of heterogeneous catalytic ozonation by cordierite-supported copper for the degradation of nitrobenzene in aqueous solution. *Environ. Sci. Technol.* 43, 2047–2053. doi: 10.1021/es803125h
- Zhuang, H., Han, H., Hou, B., Jia, S., and Zhao, Q. (2014). Heterogeneous catalytic ozonation of biologically pretreated Lurgi coal gasification wastewater using sewage sludge based activated carbon supported manganese and ferric oxides as catalysts. *Biores. Technol.* 166, 178–1186. doi: 10.1016/j.biortech.2014.05.056

**Conflict of Interest:** The authors declare that the research was conducted in the absence of any commercial or financial relationships that could be construed as a potential conflict of interest.

Copyright © 2020 Hu, Li, Nan, Yoza, Li, Zhan, Wang, Li, Guo and Chen. This is an open-access article distributed under the terms of the Creative Commons Attribution License (CC BY). The use, distribution or reproduction in other forums is permitted, provided the original author(s) and the copyright owner(s) are credited and that the original publication in this journal is cited, in accordance with accepted academic practice. No use, distribution or reproduction is permitted which does not comply with these terms.